Skeleton Dislocation Model for Geometric Optical Illusions

Kokichi Sugihara
Graduate School of Advanced Mathematical Sciences
Meiji University
JST, CREST
4-21-1 Nakano, Nakano-ku, Tokyo 164-8525, Japan
Email: kokichis@isc.meiji.ac.jp
Telephone: +81-3-5343-8366

***Abstract*—We propose a mathematical model for geometric optical illusions, in which optical illusions are explained by skeleton dislocations in blurred images. We first observe by computational experiments with Voronoi diagrams that the skeletons of figures consisting of thin lines are dislocated when the images are blurred, and next consider the relations between the dislocations and geometric optical illusions. We can see that many classic illusions can be explained by this mathematical model in a unifying manner.**

I. Introduction

Optical illusions are phenomena in which what we see are different from physical reality, and there are a wide range of variations. Among them, the historically oldest class is geometric optical illusions in which the sizes and orientations of geometric objects are perceived differently from the actual sizes and orientations. Typical examples include the Müller-Lyer illusion, in which two line segments of the same length appear as if they have different lengths, and the Zöllner illusion, in which parallel lines appear to be non-parallel [5], [7].

Many studies have been done to explain this class of illusions. Empirically it is observed that local orientations of geometric elements mislead perceived global orientations, and acute angles are apt to be perceived larger than the actual angles. These observations explain some of geometric optical illusions. Mathematical models have also been proposed by many researches. For example, Fermüller and Malm [3] argued that orientation illusions such as Poggendorff illusion and the Café Wall illusion can be explained by the biases of locations of edges due to finite resolution of retinal images. Arai and Arai [1] argued that illusion components can be extracted by the wavelet-type decomposition of images and that the strengths of illusions can be controlled by the addition and subtraction of those components.

In this paper, we propose a computational model of geometric optical illusions using computational-geometry tools such as the Voronoi diagram and the medial axis. We concentrate on figures composed of thin lines. We study how their skeletal structures change when the figures are blurred, and compare the changes with our perception of illusion figures.

Fermüller and Malm [3] also argued about the relation of image blurring with the optical illusions, but they studied boundaries between two different gray-label regions. In this paper, on the other hand, we concentrate on figures composed of thin lines.

The structure of the paper is as follows. In Section 2 we review a robust method for extracting the medial axis and skeleton using the Voronoi diagrams. In Section 3, we observe how the skeleton of figures is dislocated when the images are blurred. In Section 4, we associate the illusion phenomena and the dislocation of the skeleton, and show typical optical illusions, including the Müller-Lyer illusion, the Zöllner illusion and Hering illusion, can be explained by this model in a unifying manner.

II. Robust Extraction of Skeletons

Let $X \subseteq \mathbf{R}^2$ be a connected region in the plane, and let ∂X denote the boundary of X. We assume that X is closed, that is, $\partial X \subseteq X$. Let $c(p,r)$ denote the circle centered at $p \in \mathbf{R}^2$ with radius $r \geq 0$. We define $M(X)$ as the set of all center points p such that the maximal circle $c(p,r)$ in X touches ∂X at least at two points:

$$M(X) = \{p \in \mathbf{R}^2 \mid c(p,r) \subseteq X \text{ and } |c(p,r) \cap \partial X| \geq 2 \text{ for some } r > 0\}, \quad (1)$$

where $|Y|$ represents the number of elements in set Y. We call $M(x)$ the *medial axis* of X [8]. The medial axis of X can be regarded as a skeletal structure of the figure X.

For two points p and q we denote by $||p-q||$ the Euclidean distance between p and q. Let $S = \{p_1, p_2, \ldots, p_n\}$ be a set of n points in the plane. For $p_i \in S$, we define

$$R(S;p_i) = \bigcap_{p_j \in S, p_j \neq p_i} \{p \in \mathbf{R}^2 \mid ||p-p_i|| < ||p-p_j||\}. \quad (2)$$

A point in $R(S;p_i)$ is nearer to p_i than to any other points in S. We call $R(S;p_i)$ the *Voronoi region* of p_i with respect to S. The plane is partitioned into $R(S;p_1), R(S;p_2), \ldots, R(S;p_n)$ and their boundaries. We call this partition the *Voronoi diagram* for S [12]. We denote the Voronoi diagram for S by $\mathrm{Vor}(S)$. The boundary edges of two Voronoi regions and called *Voronoi edges*, and the common terminal points of three or more Voronoi edges are called *Voronoi points*. The elements of S are called the *generators* of $\mathrm{Vor}(S)$. The Voronoi diagram is the partition of the plane into regions according to the nearest generators. Hence, in particular, a Voronoi edge is in

equal distance from the two generators associated with the side Voronoi regions.

The medial axis of X can be computed approximately using the Voronoi diagram in the following way [12]. First, we replace the boundary ∂X with sequences of points densely located along ∂X, and let the resulting set of points be denoted by $G(X)$. We abbreviate $G(X)$ simply by G if X is clear in the context. Two points p and q in G are said to be adjacent if they are located next to each other along ∂X.

Next we compute the Voronoi diagram for the generator set G with respect to the Euclidean distance. Let the resulting Voronoi diagrams be $\mathrm{Vor}(G)$, and let E be the set of all Voronoi edges in $\mathrm{Vor}(G)$.

Finally we collect from E those Voronoi edges whose two sides generators are not adjacent to each other on the boundary ∂X and which are included in X. Let the resulting set of Voronoi edges be E^*. Then, E^* can be regarded as an approximation of the medial axis $M(X)$.

Fig. 1 shows an example of this computation of the medial axis. Let X be the region represented by the black area in Fig. 1(a). We replace ∂X with a number of points and construct the Voronoi diagram for those points. The resulting Voronoi diagram is as shown in Fig. 1(b), where all the edges in E as drawn. Removing the edges which are outside of X or whose side generators are adjacent, we get the diagram shown in Fig. 1(c), where the original figure and the edges in E^* are shown; we can regard E^* as an approximation of the medial axis of X. This is a well-known method for computing the medial axis of a figure using the Voronoi diagram.

However, as we can see in Fig. 1(c), the medial axis has many branches corresponding to small undulation of the boundary shape, and hence the medial axis in general is a mixture of the global structure and the tiny local structure. So next we want to extract only the basic part of the structure that represents the global shape of X.

Many indices have been proposed to evaluate the importance of the points on the medial axis [13], [15]. Among them, the one proposed by Sakai and Sugihara [14] is the most successful because it can extract the global structure in a robust manner by guaranteeing the topological structure of the original figure. Their index is defined in the following way.

Let $M(X)$ be the medial axis of the figure X, and p be a point in $M(X)$. Let $Q(p)$ be the set of points on the boundary ∂X at which the maximal circle $c(p,r)$ in X touches ∂X. From the definition of the medial axis, we get $|Q(p)| \geq 2$. Next for q and $q' \in Q(p)$, let $l(q,q')$ be the distance between q and q' measured along the boundary ∂X. Because ∂X is composed of one or more closed curves, there are two paths between q and q' if they belong to the same curve. We take the shorter one to measure $l(q,q')$. So if q and q' are on the same connected component of ∂X, $l(q,q')$ will be a positive real, whereas if q and q' are on mutually different components, $D(q,q') = \infty$.

Let $p \in M(X)$. We define

$$D(p) = \max_{q,q' \in Q(p)} \{l(q,q')\}. \tag{3}$$

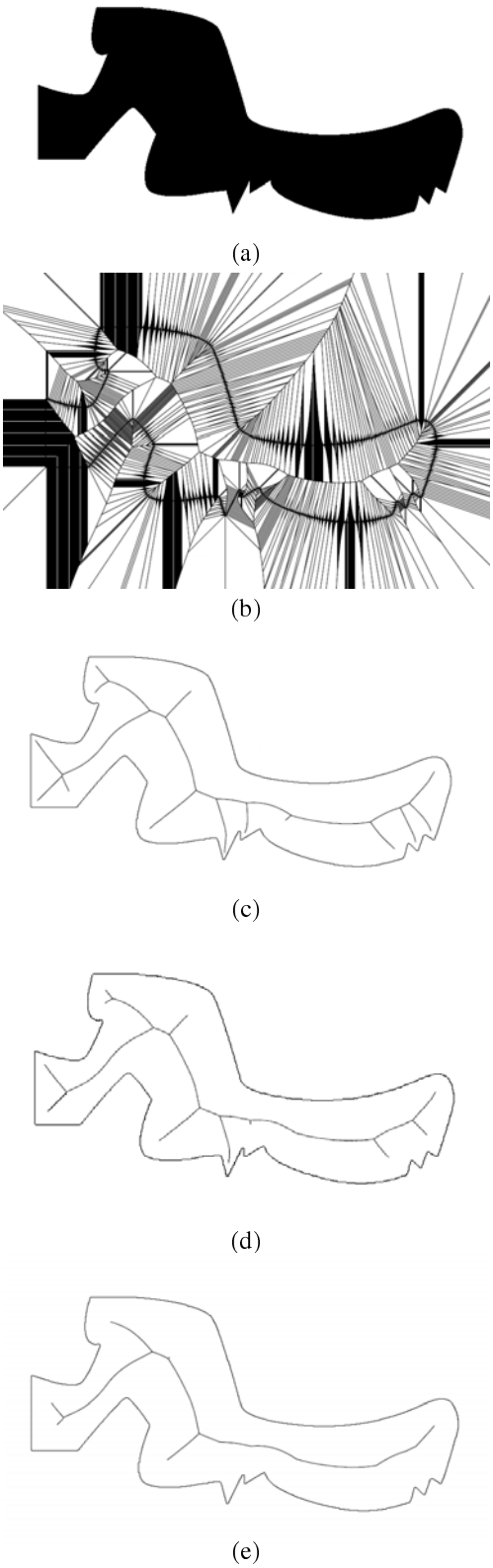

Fig. 1. Extraction of skeletons of a figure through the Voronoi diagram: (a) figure; (b) Voronoi diagram for the boundary points; (c) medial axis; (d) skeleton based on a small threshold; (e) skeleton based on a large threshold.

$D(p)$ can be considered an index that shows the importance of the point p in the medial axis. In other word, if $D(p)$ is small,

the point p corresponds to a local structure of the medial axis, which is caused by a tiny undulation of the boundary. If $D(p)$ is relatively large, on the other hand, p corresponds to a global structure of the medial axis. So we define for real $t > 0$,

$$M_t(X) = \{p \in M(X) \mid D(p) \geq t\}. \tag{4}$$

If t is small, $M_t(X)$ contains details of the medial axis, and as t becomes larger, $M_t(X)$ represents only global structure of the medial axis. We call $M_t(X)$ the *skeleton* of X with respect to the importance threshold t. In Fig. 1, (d) shows $M_t(X)$ for a small t, and (e) shows $M_t(X)$ for a large t. We can see that the skeleton in Fig. 1(e) corresponds to a global structure of the original figure X.

In this paper, we use the skeleton defined as above as a tool to model geometric optical illusions.

We would like to give a remark on the actual computation of the Voronoi diagrams. Algorithms for computing the Voronoi diagrams are well studied from a theoretical view points and many efficient algorithms were proposed. They include the plane-sweep method [4], the divide-and-conquer method [9], the lift-up method [2] and the incremental method [11], to mention a few. However, we have to be careful about numerical errors, because numerical errors cause inconsistency and can make correct algorithms to fail. So we need robust computer software to guarantee the consistency in the course of algorithm execution. For that purpose there are two powerful approaches; one is the exact computation approach [16] and the other is topology-oriented approach [17]. In this paper we use the exact-computation software for the computational experiments.

III. Dislocation of Skeletons due to Image Blurring

Let X be a region in the plane. We consider X as a black figure placed on a white background. Our retina has a limited resolution, and hence when we see a figure, the perceived image is blurred to a certain extent. In this section we observe how the location of the skeleton is shifted when the image is blurred.

In order to present our idea, let X be the figure composed of two line segments mutually crossing at their middle points in a general angle, as shown in Fig. 2(a). Let us define function $f_X(p)$ for point $p \in \mathbf{R}^2$ in the following way.

$$f_X(p) = \begin{cases} 1 & \text{if } p \in X, \\ 0 & \text{if } p \neq X, \end{cases} \tag{5}$$

and call $f_X(p)$ the *image functions* of X. We define another function $g_X(p)$ as

$$g_X(p) = \frac{1}{2\pi\sigma^2} \int_{q \in \mathbf{R}^2} f_X(q) \exp\left(\frac{||p-q||^2}{2\sigma^2}\right) \mathrm{d}q, \tag{6}$$

where $||p-q||$ represents the Euclidean distance between p and q, and σ^2 represents a variance parameter. The value of $g_X(p)$ is the weighted average of the image function around p with the Gaussian function centered at p as the weight. The function $g_X(p)$ obtained from the image function $f_X(p)$ in Fig. 2(a) is represented in Fig. 2(b), where the value of $g_X(p)$ is represented by the gray value.

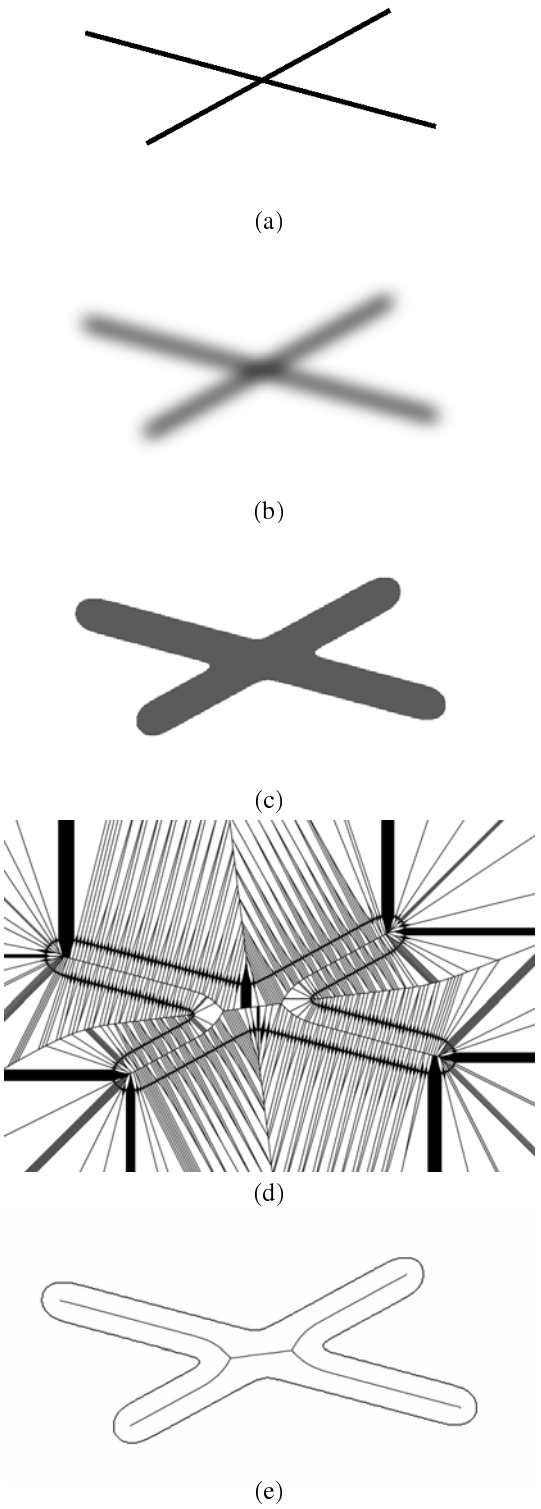

Fig. 2. Skeleton dislocation due to image blurring: (a) figure; (b) blurred image; (c) binarization of the blurred image; (d) Voronoi diagram for the boundary points; (e) skeleton.

Note that $f_X(p)$ represents a black figure on a white background, and $g_X(p)$ is its blurred image. Actually the sharp boundary between the black and the white is replaced with

smoothly changing gray regions. The mapping from $f_X(p)$ to $g_X(p)$ is called the *Gaussian filter* [10].

Next we fix some threshold $B, 0 < B < 1$, and binarize $g_X(p)$ to get the third function $h_X(p)$ by

$$h_X(p) = \begin{cases} 1 & \text{if } g_X(p) \geq B, \\ 0 & \text{if } g_X(p) < B. \end{cases} \tag{7}$$

For the example figure in Fig. 2(b), we get the binary image $h_X(p)$ as shown in (c). Then we get the Voronoi diagram for its boundary points as shown in (d) and the skeleton as shown in (e).

Because the original figure consists of thin lines, if we do not blur the image, the associated skeleton is almost the same as the original figure. On the other hand, if we blur the image the associated skeleton changes as in the example shown in Fig. 2(e). Let us call this shift of the location of the skeleton the *dislocation* of the skeleton due to blurring.

The dislocation of the skeleton is a common phenomenon when we blur a figure composed of thin lines. We next apply the dislocation phenomena to explain geometric optical illusions.

IV. Optical Illusions Described by Skeleton Dislocation

In this section, we will show several typical optical illusion caused by figures consisting of thin lines can be explained by the skeleton dislocation phenomena in a unifying manner.

A. Müller-Lyer illusion

Fig. 3(a) shows one of the most famous geometric optical illusions called the Müller-Lyer illusion. In this figure the two horizontal line segments are of the same length, but the one with outer allows appears longer than the other. A prevailing explanation of this illusion is "line perspective" by Gregory [6]. He associated the line segment having outer arrows with the farthest corner of a rectangular room, and the line segment having inner arrows with the nearest corner of a rectangular building, and he argued that these depth interpretations distort the apparent lengths.

On the other hand, we can explain the Müller-Lyer illusion by the skeleton dislocation in the following way. We blur the original figure in Fig. 3(a) and get the blurred image Fig. 3(b). Next, we construct the Voronoi diagram for the boundary points of the binarized image as in Fig. 3(c), and get the skeleton as in Fig. 3(d). We can observe that the horizontal parts of the two skeletons differ much in their lengths; the one with outer arrows has longer horizontal part than the other. Thus, the Müller-Lyer illusion can be explained by the dislocation of the skeletons.

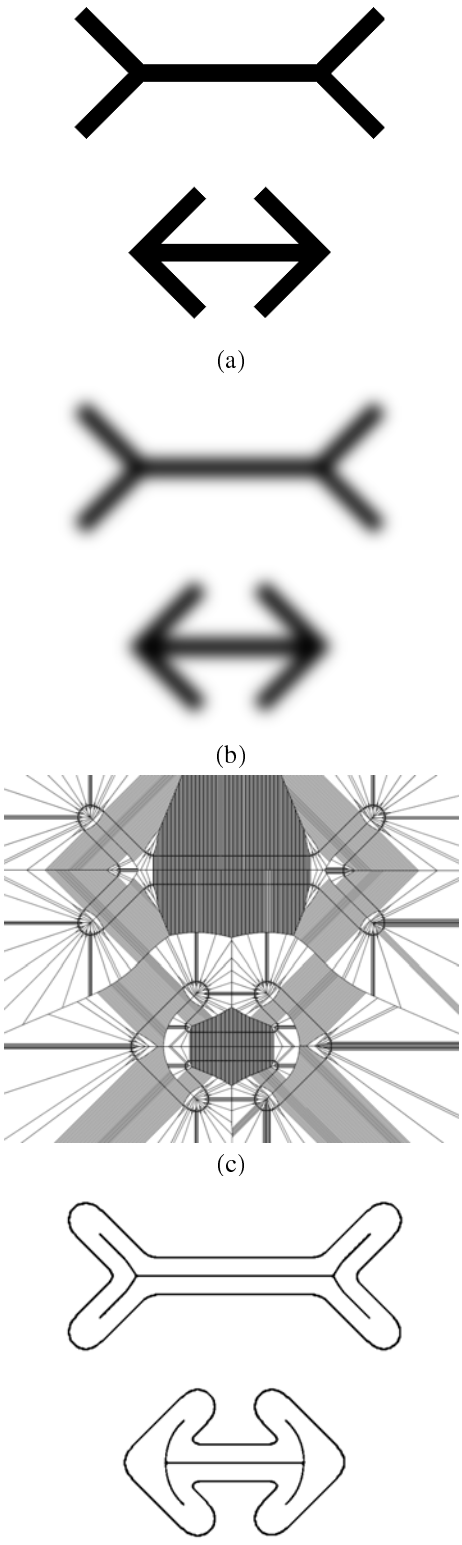

Fig. 3. Müller-Lyer illusion: (a) original figure; (b) blurred image; (c) Voronoi diagram for the boundary points of the binarized image; (d) skeleton of the blurred figure.

B. Zöllner illusion

Another famous and classic illusion is Zöllner illusion shown in Fig. 4, where the horizontal lines are parallel but they apperar to be slanted in alternating directions.

We call the horizontal lines the *target lines*, and the short slanted lines the *inducing lines*; the including lines seem to induce the perceived orientation of the target lines.

Let l_1 and l_2 be two parallel lines in the plane. Suppose that l_1 and l_2 are rotated slightly and their orientations change. If

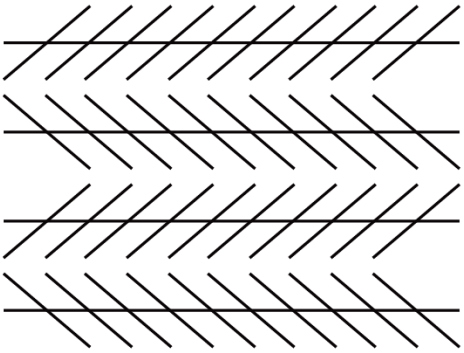

Fig. 4. Zöller illusion.

both l_1 and l_2 are rotated clockwise, we say that the orientation changes have the *same polarity*. Similarly, if they are both rotated counterclockwise, we say that their orientation changes have the *same polarity*. On the other hand, if one is rotated clockwise and the other is rotated counterclockwise, we say that their orientation changes have *opposite polarities*.

In Zöllner illusion, the adjacent target lines are perceived in such a way that their orientation changes have opposite polarities.

This illusion is usually explained as a visual phenomena in which acute angles are apt to be perceived larger than the actual values. On the other hand, we can explain this illusion by skeleton dislocation in the following way.

Let us concentrate on one target line of the Zöllner illusion figure in Fig. 4. We blur the original figure and get the blurred image as shown in Fig. 5(a). The Voronoi diagram for the boundary points of the binarized image is obtained as in Fig. 5(b), and the skeleton is obtained as in Fig. 5(c). Fig. 5(d) shows an overlay of the skeleton with the fatten inducing lines. This figure represents how the target line is dislocated by image blurring. The dislocated skeleton segments are slanted in the same direction as the perceived direction, that is, the orientation change in the skeleton dislocation has the same polarity as the perceived orientation change. Thus, the Zöllner illusion can be explained by the skeleton dislocation.

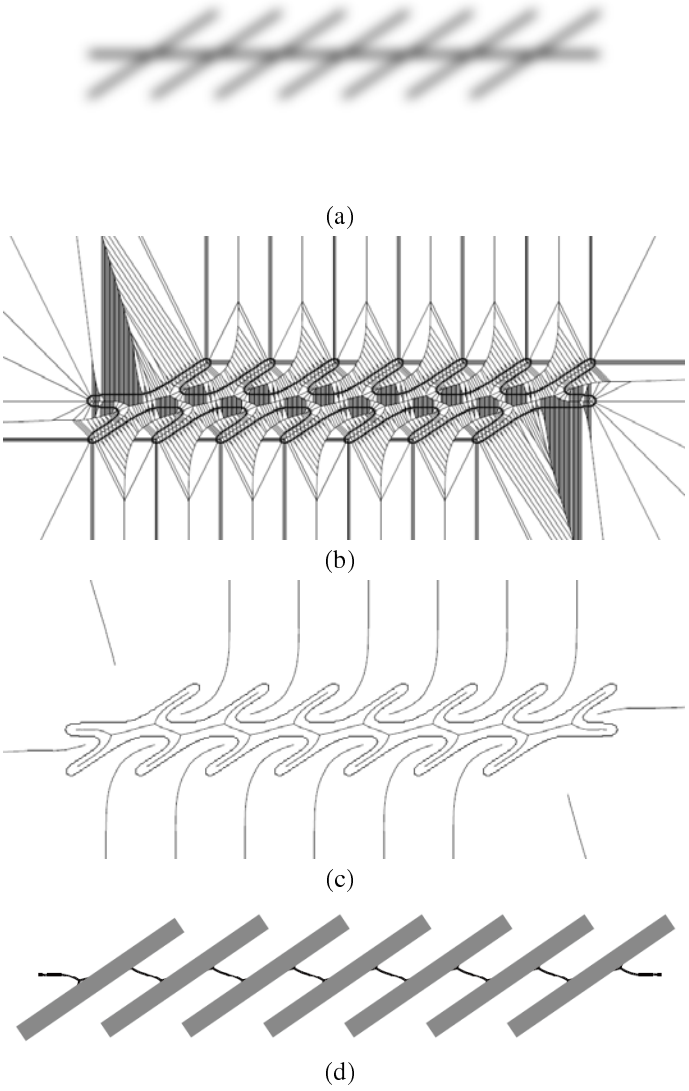

Fig. 5. Skeleton dislocation for the Zöllner illusion: (a) blurred image of one target line of the Zöllner illusion figure in Fig. 4; (b) Voronoi diagram for the boundary points of the binarized image; (c) skeleton; (d) overlay of the skeleton with the fatten inducing lines.

C. Hering illusion

Fig. 6 shows the Hering illusion. The two long lines appear to be curved although they are exactly horizontal and parallel. We call these two horizontal lines the *target lines*, and the two bundles of radial lines the *inducing lines*. Usually this illusion is also explained by the phenomenon that acute angles are apt to be perceived larger than the actual angles.

We can explain the Herring illusion also by the skeleton dislocation. Let us concentrate on the upper part of the Herring illusion figure. We get a blurred image as shown in Fig. 7(a), and the Voronoi diagram for the boundary points of the binarized image as shown in Fig. 7(b). The skeleton is obtained as shown in Fig. 7(c), and the overlay of the skeleton with the fatten inducing lines is as shown in Fig. 7(d). The skeleton segments corresponding to the target line are slanted in the same orientation as the perceived local orientations of the target line. That is, the orientation changes have the same polarities as the perceived orientations. Thus, the Herring illusion can also be explained by the skeleton dislocation.

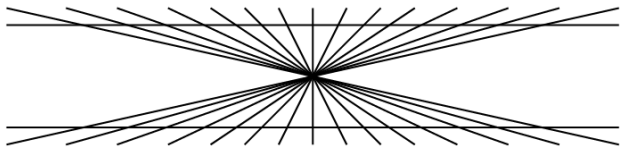

Fig. 6. Herring illusion.

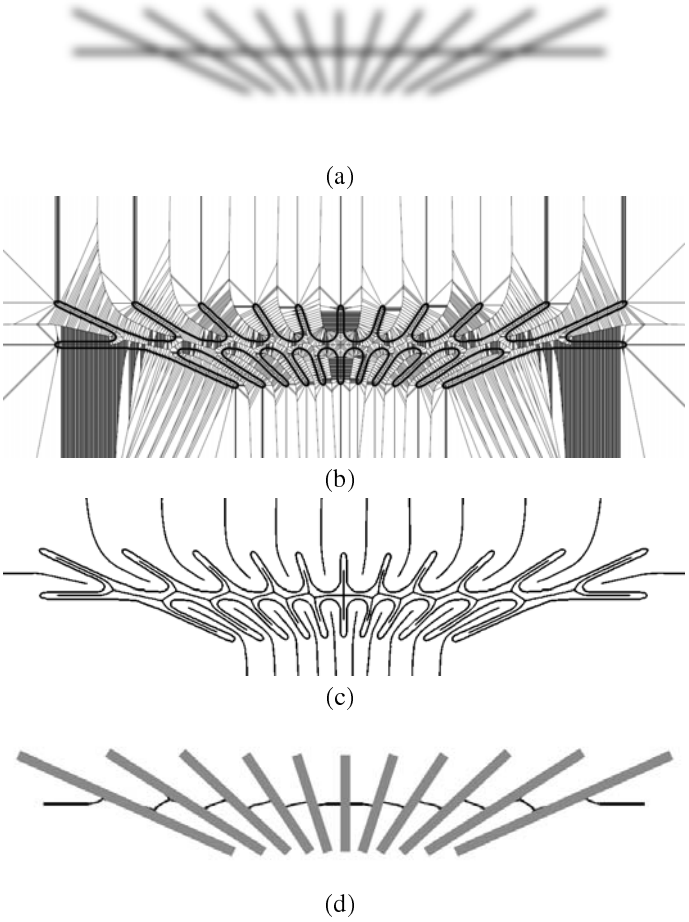

Fig. 7. Skeleton dislocation for the Hering illusion: (a) blurred image of the upper part of the Hering illusion figure in Fig. 6; (b) Voronoi diagram for the boundary points of binarized image; (c) skeleton; (d) overlay of the skeleton with fatten inducing lines.

D. Ponzo illusion

Fig. 8(a) shows the Ponzo illusion. The two circles are of the same size, but the left one appears larger than the right one. This illusion is usually explained by the line perspective; the two lines give an impression that the left part is farther than the right part from the viewer, and consequently the left circle is farther than the right circle, giving the difference of the perceived sizes due to the size constancy.

We blur the Ponzo figure and get the blurred image as shown in Fig. 8(b). The Voronoi diagram for the boundary points of the binarized image is obtained as in Fig. 8(c), and the skeleton is obtained as in Fig. 8(d). The skeleton corresponding to the left circle is larger in the vertical direction than that corresponding to the right circle. Thus, the skeleton dislocation explains the Ponzo illusion.

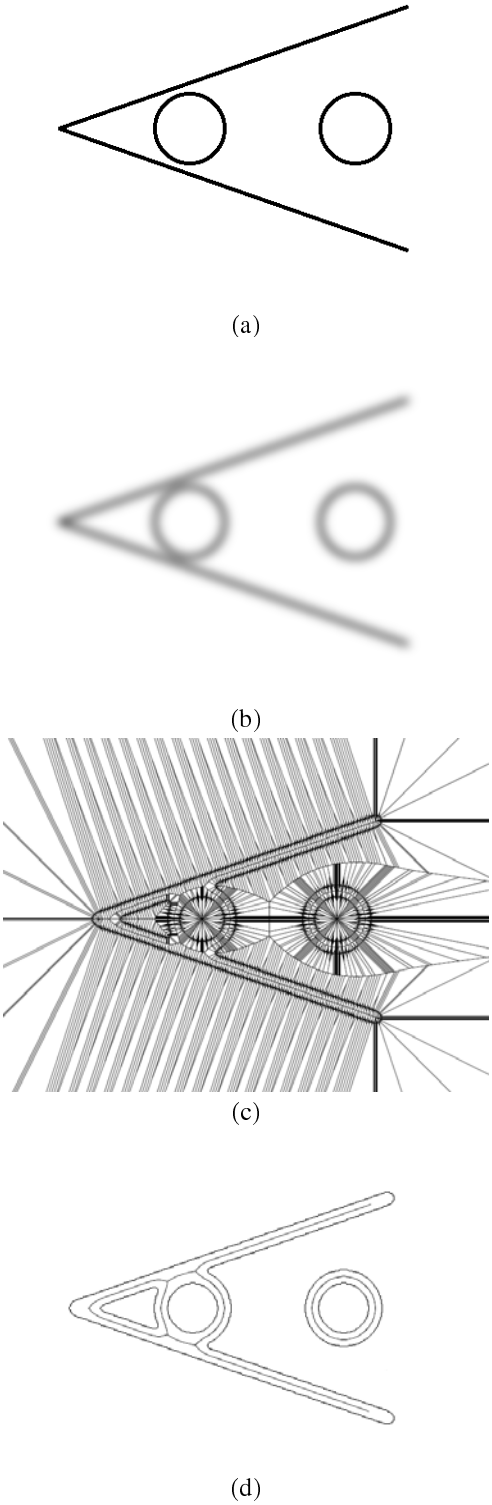

Fig. 8. Ponzo illusion: (a) original figure; (b) blurred image; (c) Voronoi diagram for the boundary points of the binarized image; (d) skeleton of the blurred image.

V. Concluding Remarks

In this paper we observed the dislocation phenomena of the skeleton of figures composed of thin lines according to the image blurring, and apply it to explain some of typical geometric optical illusions in a unifying manner. We adopted the three typical optical illusions: the Müller-Lyer illusion, the Zöllner illusion, the Herring illusion and the Ponzo illusion.

The same explanation is also possible to many other geometric illusions, including the Wundt illusion, Ehrenstein illusion, the Obrison illusion and Judd illusion.

Readers might feel that the blurring used in this paper is too much exaggerated than the blurring that actually occur in our retina and brain neurons. However, there is still possibility that this amount of large blurring actually occurs in our visual perception system. Optical illusion in general is irrational and illogical in the sense that, even if we know the physical truth, we perceive the sizes and orientations incorrectly. These phenomena suggest that our brain contains a large part or irrational information processing components, and they might use very rough data such as highly blurred images. Actually, the skeleton dislocation theory proposed in this paper should be investigated from anatomical and experimental aspects in order to see whether it is actually happening in the brains. This is the most important problem for future.

ACKNOWLEDGMENT

The work is supported by the Grants-in-Aid for Challenging Exploratory Research No. 24650015 and Scientific Research (B) No. 24360039 of MEXT.

REFERENCES

[1] H. Arai and S. Arai: Framelet analysis of some geometric illusions. *Japan Journal of Industrial and Applied Mathematics*, vol. 27, pp. 23–46, 2010.

[2] K. Q. Brown: Voronoi diagrams from convex hulls. *Information Processing Letters*, vol. 9, pp. 223–228, 1979.

[3] C. Fermüller and H. Malm: Uncertainty in visual processes predicts geometrical optical illusions. *Vision Research*, vol. 44, pp. 727–749, 2004.

[4] S. Fortune: A sweepline algorithm for Voronoi diagrams. *Algorithmica*, vol. 2, pp. 153–174, 1987.

[5] T. Goto and H. Tanaka: *Handbook of the Science of Illusion* (in Japanese). University of Tokyo Press, tokyo, 2005.

[6] R. L. Gregory: *Eye and Brain*, McGraw-Hill, New York, 1966.

[7] A. Kitaoka: *Introduction to Visual Illusion* (in Japanese). Asakura-Shoten, Tokyo, 2010.

[8] D. T. Lee: Medial axis transformation of a planar shape. *IEEE Transaction of Pattern Analysis and Machine Intelligence*, vol. PAMI-4, pp. 363–369, 1982.

[9] D. T. Lee and B. J. Schacher: Two algorithms for constructing the Delaunay triangulation. *International Journal of Computer and Information Sciences*, vol. 9, pp. 219–242, 1980.

[10] D. Marr: *Vision*, W. H. Freeman and Company, New York, 1982.

[11] T. Ohya, M. Iri and K. Murota: Improvements of the incremental method for the Voronoi diagram with computational comparison of various algorithms. *Journal of the Operations Research Society of Japan*, vol. 27, pp. 306–336, 1984.

[12] A. Okabe, B. Boots, K. Sugihara and S.-N. Chiu: *Spatial Tessellations —Concepts and Applications of Voronoi Diagrams*. Second Edition, John Wiley and Sons, Chichester, 2000.

[13] S. M. Pizer, W. R. Oliver and S. H. Bloomberg: Hierarchical shape description via the multiresolution symmetric axis transformation. *IEEE Trans. Pattern Anal. & Mach. Intell.*, vol. PAMI-9, no. 4, pp. 505–511, 1987.

[14] H. Sakai and K. Sugihara: Stable and topology-preserving extraction of medial axes. *Proceedings of the 3rd International Symposium on Voronoi diagrams in Science and Engineering*, Banff Center, July 2-5, 2006, pp. 40–47.

[15] D. Shaked and A. M. Bruckstein: Pruning medial aces. *Computer Vision and Image Understanding*, vol. 69, pp. 156–169, 1998.

[16] K. Sugihara: A simple method for avoiding numerical errors and degeneracy in Voronoi diagram construction. *IEICE Transactions on Fundamentals of Electronics, Communications and Computer Sciences*, vol. E75-A, pp. 468–477, 1992.

[17] K. Sugihara and M. Iri: A robust topology-oriented incremental algorithm for Voronoi diagrams. *International Journal of Computational Geometry and Applications*, vol. 4, pp. 179–228, 1994.